Available online at www.sciencedirect.com
ScienceDirect
Procedia Engineering 102 (2015) 749 – 758
Procedia Engineering
www.elsevier.com/locate/procedia

The 7th World Congress on Particle Technology (WCPT7)

"Laser sintering of unimodal distributed glass powders of different size"

"Daniele Sofia, Mirko Granese, Diego Barletta, Massimo Poletto" *

"Department of Industrial Engineering, University of Salerno, Via Giovanni Paolo II, 132, Fisciano (SA) 84084, Italy"

Abstract

In the present paper heat exchange rates for selective laser melting/sintering (SLM/SLS) of glass beads were evaluated. Experiments were carried out with a nominal 40W CO_2 laser, on samples characterized by different particle size distributions within16 and184 μm, and different laser scan speeds (1-30 mm s^{-1}). The energy required for the sintering process depends on the particle size. In particular, part of the energy supplied by the laser beam is dispersed by different mechanisms of energy transfer. These quantities were estimated to evaluate the process effectiveness in particle melting or sintering. On this purpose the energy balance was solved by combining experimental data and exchange coefficients calculated from known empirical correlations. The amount of the molten mass changes with particle size and maximum is observed for the sample with average particle size of 48 μm. The increase of the molten mass between 16 μm and 48 μm is 24% at a scan speed of 1 mm s^{-1} and it is 47% at a scan speed of 5 mm s^{-1}.

Selection and peer-review under responsibility of Chinese Society of Particuology, Institute of Process Engineering, Chinese Academy of Sciences (CAS)

"Keywords: Selective laser sintering, Selective laser melting, 3D printing, rapid prototyping, particle size distribution"

1. Introduction

Selective laser sintering (SLS) fits into the class of methods for rapid prototyping and 3D printing. It is an emerging technology that allows to craft artefacts with excellent mechanical properties starting from powders of

* Corresponding author. Tel.: +39-089-964132; fax: +39-089 964057.
E-mail address: mpoletto@unisa.it

Selection and peer-review under responsibility of Chinese Society of Particuology, Institute of Process Engineering, Chinese Academy of Sciences (CAS)
doi:10.1016/j.proeng.2015.01.180

different compositions (polymeric, metallic or ceramic), and by selectively heating powders to the sintering point with a laser beam. Differently from sintering [1], selective laser melting (SLM) is an alternative laser technology in which the material is brought to the molten state,. The interaction time between the material and the laser beam is in general very short (<1 s) to minimize chemical and physical interactions produced by the heating. In SLS, it is possible to use powders of the same type (direct sintering) or mixtures of different powders, in which generally one of them acts as a binder for the higher temperature melting (indirect sintering). The great interest from the industrial point of view is related to the possibility of rapidly obtain a prototype of the artefact and be able to produce high temperature resistant components, piezoelectric sensors and actuators [2], and biocompatible applications in the medical field [3]. The process description from the thermal point of view requires to contemplate simultaneously several mechanisms such as phase change and heat transfer by radiation, convection and conduction. According to the most common approach[4], the energy balance should include radiation from the heated bed, convection from the solids surface to the gaseous environment, conduction to powder surrounding the laser heated particles. The physical properties involved may change considerably and quickly during the process, however often simplifying assumptions are adopted. In general, increasing the energy transferred by laser increases the strength of the structure obtained, but it also produces a volume contraction of the sintered material which reduces the precision of the final object [5].There are many models in the literature, which refer to the Fourier's heat transfer equation, such as those proposed by Carslaw et al. [6], who have focused their study on the boundary conditions. Other models consider the effect of the shrinkage of the powder and the fluid flow within the molten material [7]. Other authors consider the change of surface properties during irradiation [8]. In the present work, a study on the effect of the particle size distribution on the amount of energy actually used for particle melting is proposed. Also the effect of the laser scanning speed is considered and the effect of temperature on the effective thermal conductivity of the powders.

Nomenclature

A_m	irradiating area of the melted material (m^2)
A_p	projected area of the melted material (m^2)
c_p	specific heat (J $kg^{-1}K^{-1}$)
d_p	particle diamenter (m)
d_s	mean Sauter diamenter (m)
k_e	effective thermal conductivity (W m^{-1} K^{-1})
k_s	solid thermal conductivity (W m^{-1} K^{-1})
k_g	gas thermal conductivity (kg m^{-3})
m	mass (kg)
Q_L	heat power laser (W)
Q_M	heat power melting (W)
Q_{cond}	heat power conduction (W)
Q_{conv}	heat power convection (W)
Q_{irr}	heat power irradiation (W)
t	time (s)
T	temperature (K)
T_a	ambient temperature (K)
T_m	melt temperature (K)
x	Cartesian coordinate (mm)

Greek letters

ε	emissivity of surface
ρ	bulk density (kg m^{-3})
ρ_s	solid density (kg m^{-3})
σ	Stefan-Boltzmann constant (W m^{-2} K^{-4})
ϕ	empirical coefficient
μ	solid fraction ratio ρ/ρ_s
λ	latent heat of vaporization

2. Experimental

2.1. Apparatus

The apparatus used for the process consists in a 40 W CO_2 tube, emitting a laser beam at a wavelength of 10.6 μm and with a spot size of 100 micron diameter. A couple of mirrors moving on the x-y plane allow to place the laser spot on any point of the flat surface of the powder sample. The laser scan velocity range can be adjusted between 1 mm s^{-1} and 100 mm s^{-1}. The nominal laser power of 40 W is sufficient for the melting or sintering process of several ceramic materials. Three dimensional objects might in principle be obtained by lowering the powder sample and covering it with a new powder layer, thin enough to be reached in its thickness by the laser beam, for a total working volume of 100 × 100 × 50 mm. In this paper, however, only the results obtained by working on a single powder layer will be addressed.

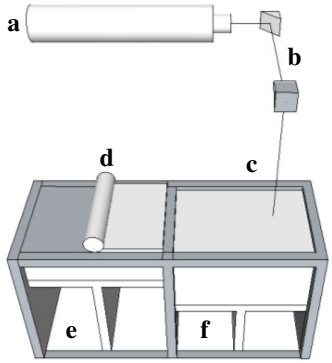

Figure 1. Apparatus of laser sintering a) laser tube; b) scanning mirrors moving in x and y directions; c) laser beam; d) powder spreading roller; e) powder reservoir (upward movement); f) working volume (downward movement).

2.2. Materials

Three batches of glass beads with a wider particle size distribution (<50 µm; 10 µm - 100 µm; 100 µm - 200 µm) were sieved in order to obtain samples characterized by narrow particle size distributions. Mean Sauter diameters, d_s, the particle ranges of the original batches and the undersize and oversize sieve meshes used to produce each sample are reported in Table 1. Powders sieved samples were characterized using a LEO 420 Scanning Electron Microscope (SEM) and a Malvern Mastersizer 2000 laser diffraction based particle size analyzer with a Hydro 2000 wet dispersion accessory. The particle size distributions of the sieved samples are reported in Figure 2. The density of the powder material, a soda-limestone glass, was measured experimentally in helium Pycnometry and it is equal to 2500 kg m^{-3}. The volumes occupied by the different powders was measured with a 25 ml pycnometer. The resulting bulk densities are reported in Table 1.

Table 1. Sauter diameters, original batch, sieve meshes used to obtain the different glass bead samples and bulk densities.

d_s, µm	Original cut size range, µm	sieved range, µm	ρ, kg m^{-3}
16	<50	< 25	1368
27	<50	25-63	1404
48	10-100	63-90	1504
86	100-200	90-125	1524
160	100-200	125-180	1536
184	100-200	180-250	1540

The material heat capacity and glass transition was characterized by means of DSC (Differential Scanning Calorimetry) using a SDT Q600 of TA Instruments. The test was carried out up to a temperature of 1200 ° C, with a heating ramp of 20 °C per minute. Figure 3 shows the response of the material to heating, the performance is consistent with the type of material (soda-limestone glass)[9].

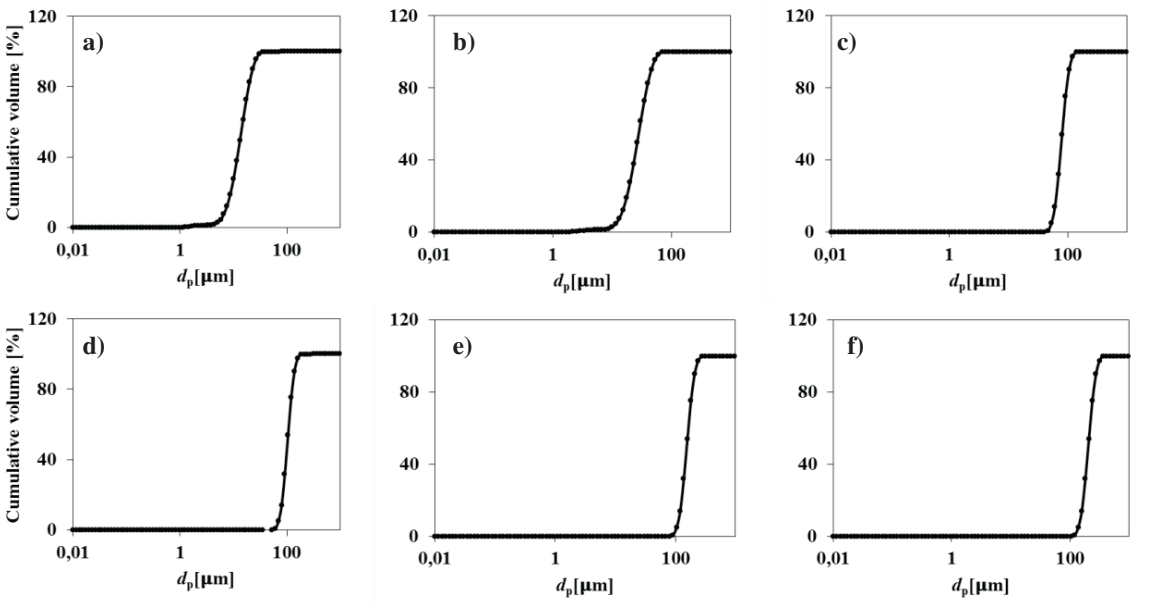

Figure 2. Particle size distribution of the glass powders after sieving. d_p: a) 16 µm, b) 27 µm, c) 48 µm, d) 86 µm, e) 160 µm, f) 184 µm.

2.3. Scanning test

The effect of the laser sintering on different sized samples (16 µm, 27 µm, 86 µm, 120 µm, 160 µm, 184 µm) was tested. samples of each material were prepared in 40 mm caps. Samples were levelled and consolidated at 2.5 kPa and two 90° twisting under a flat rotating lid. for each sample For each sample, different sintering tests were carried out at different laser scanning speeds in each of which the laser beam was continuously run in lines 10 mm long. The scan speeds used were 1, 5, 10, 15, 20, 25 and 30 mm s^{-1}. Pictures of the resulting sintering effects are reported in Figure 4. The laser scanning speed has the main effect on all samples, with larger amounts of melted material at lower speeds, corresponding to higher energy per unit distance covered by the laser bean. Slighter differences in the melted materials and in the number of resulting droplets are observed as a function of the sample particle size.

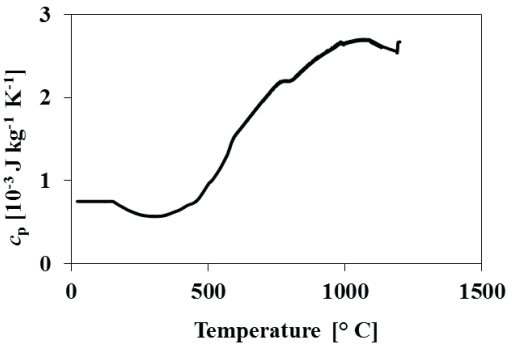

Figure 3. Specific heat capacity of the powder material (soda-limestone glass).

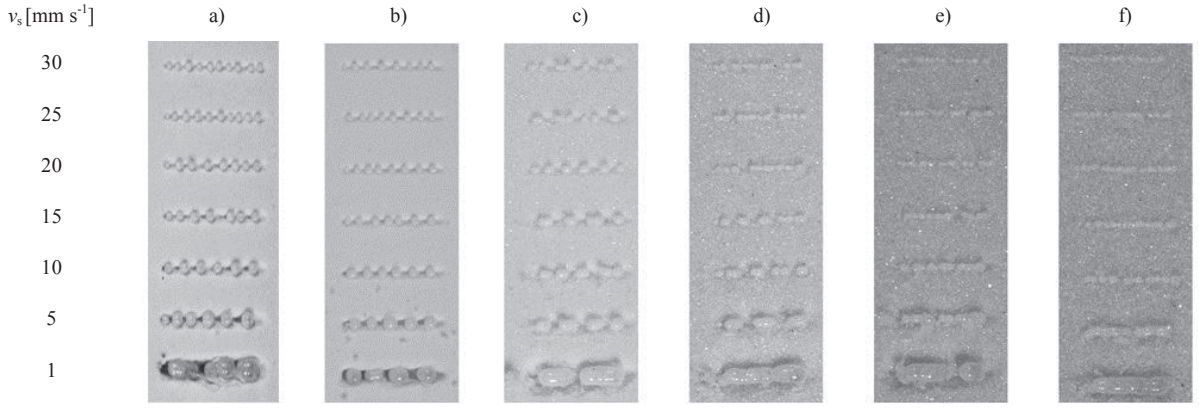

Figure 4 Effect of the laser scan velocity v_s and of the grain size of the glass beads d_s: a) 16 µm; b) 27 µm; c) 86 µm; d) 120 µm; e) 160 µm; f) 184 µm.

3. Theory

3.1. Energy balance

From the results presented above, it appears clearly that the main difference between tests is due to the different energy released by the laser to the sintered material. The longer it takes to the laser beam to complete the line the larger is the energy released to the sample, the larger is the quantity of the melted material. However, it is well known that [10] not all the released laser energy is used to melt the material since in parallel with the melting process also heat dispersion occurs by different mechanisms of heat transfer (Figure 5). In order to evaluate the relative importance of these heat dispersion mechanisms compared with the melting process, it was necessary to sketch an energy balance (eq.1). The mechanism included in this heat balance are radiation, convection and conduction. The power balance assumes the form:

$$\dot{Q}_L = \dot{Q}_M + \dot{Q}_{cond} + \dot{Q}_{conv} + \dot{Q}_{irr} \qquad (1)$$

where $\dot{Q}_L$ is the power supplied by the laser, $\dot{Q}_M$ is the power required for melting the material, $\dot{Q}_{cond}$ is the power dispersed by conduction in the powder bed, $\dot{Q}_{conv}$ is the power lost from the granular material by convection and $\dot{Q}_{irr}$ power lost from the granular material by irradiation.

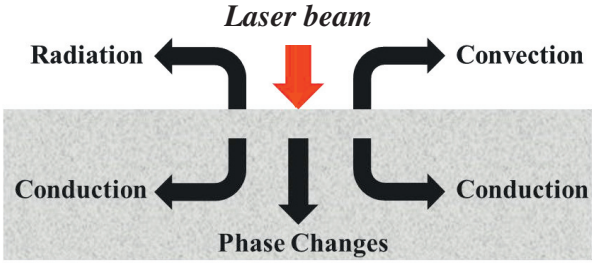

Figure 5 The mechanisms of heat transfer for the processes SLS / SLM.

An estimate of the effective energy supplied by the laser was necessary. A darkened and narrow necked bottle containing 70 g of water and a dark target for the laser was hit by the laser beam for 60 s. Assuming that the whole

energy released by the laser was converted either in latent heat of vaporization or in sensible heat for the water the effective laser power was estimated as follows.

$$\dot{Q}_{\mathrm{L}} = \frac{\left(m_{\mathrm{H_2O}}\, c_{\mathrm{p\,H_2O}}\, \Delta T + \Delta m_{\mathrm{H_2O\_vap}}\, \lambda_{\mathrm{H_2O}}\right)}{\Delta t} \tag{2}$$

where m_{H2O} is the final mass of water in the bottle, Δm_{H2O} is the mass of vaporized water. Repeated experiments were carried out to and a net laser power output of 16 W was estimated.

The power required to melt the powder material can be calculated as follows:

$$\dot{Q}_{\mathrm{M}} = \frac{1}{t_{\mathrm{line}}} \int_{T_{\mathrm{a}}}^{T_{\mathrm{m}}} m\, c_{\mathrm{p}}\, dT \tag{3}$$

where, m is the molten mass in a line, C_{p} is the specific heat capacity, T_{m} is the maximum temperature of the melt T_{a} the initial bed temperature equal to the ambient temperature and t_{line} the time required for the laser to scan the 10 mm line.

The energy dispersed by conduction in the bed was calculated using the Fourier equation in spherical geometry.

$$\dot{Q}_{\mathrm{cond}} = \left(\frac{2\pi k_{\mathrm{e}}}{\frac{1}{R_{\mathrm{m}}} \quad \frac{1}{R_{\infty}}} \right) \left(T_{\mathrm{m}} - T_{\mathrm{a}}\right) \tag{4}$$

where R_{m} is the radius of melted material and k_{e} is the effective conductivity coefficient of the powder bed .The energy lost by natural convection was calculated with the following equation:

$$\dot{Q}_{\mathrm{conv}} = h\, A_{\mathrm{p}} \left(T_{\mathrm{m}} - T_{\mathrm{amb}}\right) \tag{5}$$

where A_{p} is the horizontally projected area of the melted material .h is the convection coefficient estimated from the solution for plate cooled from above as available in [11]. The energy lost by radiation was calculated using the Stefan-Boltzmann equation under the conditions of temperature measured on the powder bed.

$$\dot{Q}_{\mathrm{irr}} = \varepsilon\, A_{\mathrm{m}}\, \sigma \left(T_{\mathrm{m}}^4 - T_{\mathrm{a}}^4\right) \tag{6}$$

where ε is the emissivity of the glass and σ is the Stefan–Boltzmann constant.

3.2. Heat conduction coefficient estimation

A proper evaluation of heat conduction required the evaluation of the proper thermal conductivity of the powder bed. An experimental procedure was used to assess on this property in a bed of 16 μm average particle size. On a sample of this powder different experiments were run by keeping the laser in a fixed position for 30 s. In each of these experiments a *K* thermocouple had been placed at a certain distance from the spot illuminated by the laser beam and at 5 mm depth, namely 3, 5, 7 and 10 mm. Figure 6 shows the sampling temperature positions. Assuming a pseudo continuous system, according to Yagui and Kunni [12], the effective bed thermal conductivity, k_{e},can be expressed as:

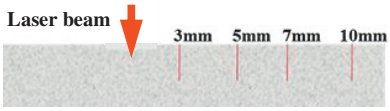

Figure 6 Sampling temperature position in the heat conduction experiment in transient temperature tests.

$$k_e = \frac{\mu k_s}{1 + \phi \frac{k_s}{k_g}} \tag{7}$$

where k_s is the conductivity of the solid material, k_g is the conductivity of the interstitial gas, air in our case, and μ is the solid fraction ratio ρ/ρ_s between the powder bulk density, ρ, and the density of the solid material, ρ_s, and ϕ is an empirical coefficient normally taken as$0.02 \cdot 10^{2(0.7-\mu)}$. According to eq. 7 the bed effective conductivity is not directly dependent on the particle size but, in our case it is indirectly dependent on it through the bed bulk density. the bed effective conductivity is also dependent on the bet temperature since the interstitial gas conductivity significantly vary with temperature. In order to estimate this effect k_g ,was calculated according to [13].

$$k_g = \frac{a T^b}{1 + \frac{c}{T} + \frac{d}{T^2}} \tag{8}$$

adopting SI units the constants are: a=3.14*10^{-4}, b= 0.77, c= -0.71, d=2121.70. As an example Figure 7a reports the resulting bed conductivity at 1800 and 1400 ° C for all the powder samples.

Assuming for this test a pseudo homogeneous model for heat conduction the Fourier equation applies:

$$k_e \frac{\partial T}{\partial t} = \rho c_p \frac{\partial^2 T}{\partial x^2} \tag{9}$$

with the initial and boundary conditions described as follows:

$$t=0 \quad \forall x \quad T=T_a \tag{10}$$
$$x=0 \quad \forall t \quad T=T_m \tag{11}$$

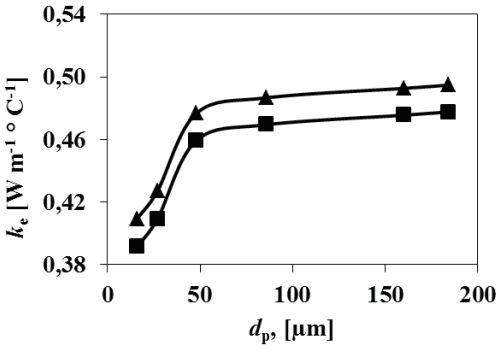

Figure 7 Effective bed conductivity k_e as a function of particle size distribution and temperature: ▲, 1800 ° C; ■, 1400 ° C

A solution to equations (9) to (11) was calculated using a finite differences numerical procedure implemented on a spreadsheet. Table 2 reports the value of the physical properties used in the numerical procedure with the corresponding units and source of data. The melt temperature was set to 1863°C, with the values of k_g 0.12 W m^{-1} K^{-1} and k_e 0.41 W m^{-1} K^{-1}. This melt temperature is the one obtained in the energy balance from the laser scanning experiment and reported in the following. Not necessarily the melted temperature should be the same in the two experiments, though, in absence of a better estimate this value was assumed as true also for this case.

Table 2. Physical properties of the material.

Name	Value	Units	Source
k_s	1	W m^{-1} K^{-1}	[10]
k_g	0.12	W m^{-1} K^{-1}	eq 8
k_e	0.41	W m^{-1} K^{-1}	eq 7
ρ	1368	Kg m^{-3}	exp.
T_a	20	°C	exp.
T_m	1863	°C	heat bal.
ρ_s	2500	Kg m^{-3}	exp.
c_p	0.002	J Kg^{-1} K^{-1}	[10]

Figure 8, reports the comparison between the experimental temperature profile and the temperature profile calculated by the thermal model at the end of 30 s heating time by using the value of k_e. calculated according to equation (7). Within the hypotheses made, the agreement between experiments and model is very good for the tested particle size distribution of 16 μm. therefore it will be assumed that the effective thermal conductivity calculated according to equation (7) is a good estimate of the effective powder bed conductivity for the powder samples of different mean size.

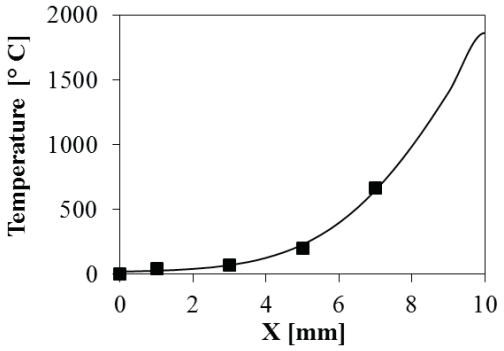

Figure 8. Comparison between the model, line, and experiments, ■, for the transient temperature tests to validate the estimate of the effective bed heat conductivity.

4. Results and discussion

4.1. Melted mass

The melted mass in each of the experiments reported in Figure 4 was measured by weighing the melt material appearing along each 10 mm line. Figure 9 shows these masses. The peak mass appears to be obtained is obtained for a particle size distribution of 48 μm. The relative increase of the mass of melted material by changing particle size is significant, in fact between 16 μm and 48 μm it can be quantified to be 24% at a scan speed of 1 mm s^{-1} and

around 47% with a scan speed of 5 mm s^{-1}. As evident in Figure 4, large differences of the melted mass are registered at different laser scan velocities.

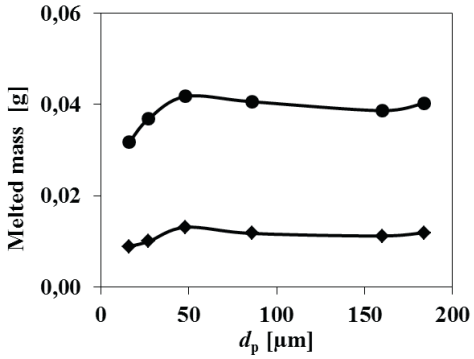

Figure 9. Melted mass evaluated by weighing for samples of different mean particle size for two scan velocities: ●, 1 mm s^{-1}, ♦ 5 mm s^{-1}

4.2. Energy dispersion

Once the mass of the melted material is experimentally determined, the energy balance defined in equations (1) to (6) allows to calculate the maximum temperatures of the melted materials T_m. appearing in all the terms on the right hand side of equation (1) Figure 10 reports these results. It shows that the temperature of the melted material decreases with the increasing mean particle size of the sample. In the same figure also the effect

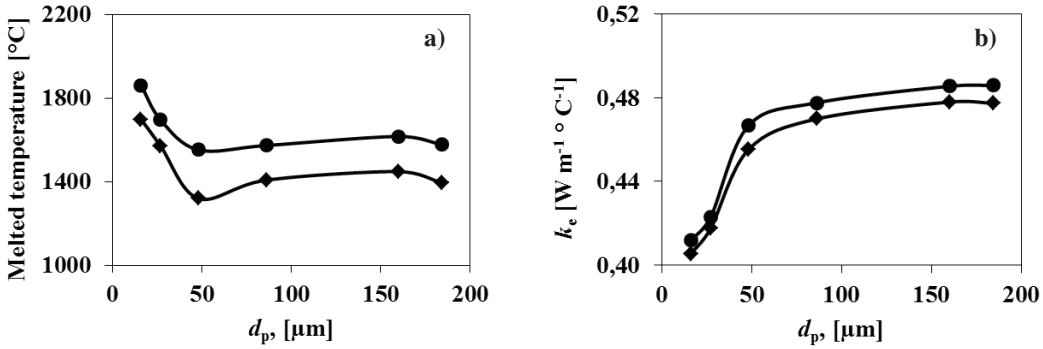

Figure 10 Temperature of the melt (a) and effective bed conductivity (b) for two scan velocities: ●, 1 mm s^{-1}, ♦ 5 mm s^{-1}.

Figure 11 shows the fractions in percent of the power dissipated by the different hypothesized mechanisms of heat dispersion together with the thermal power used for the melting of the powder. It appears that the main heat dispersion mechanism seems to be the bed conduction, in fact in all cases it is greater than the other contributions to heat dispersion. The significance of heat conduction may explain the melt temperature change with particle size. In fact an increase in particle size also correspond to the increase of k_e, and of the cooling effect of the heat dispersion that correspondingly is associated to a decrease of the melt temperature. From figure 11, it also appears that at lower scan velocities the heat dispersion has a greater relevance than at high laser scan rates due to the lower temperatures of the melted materials.

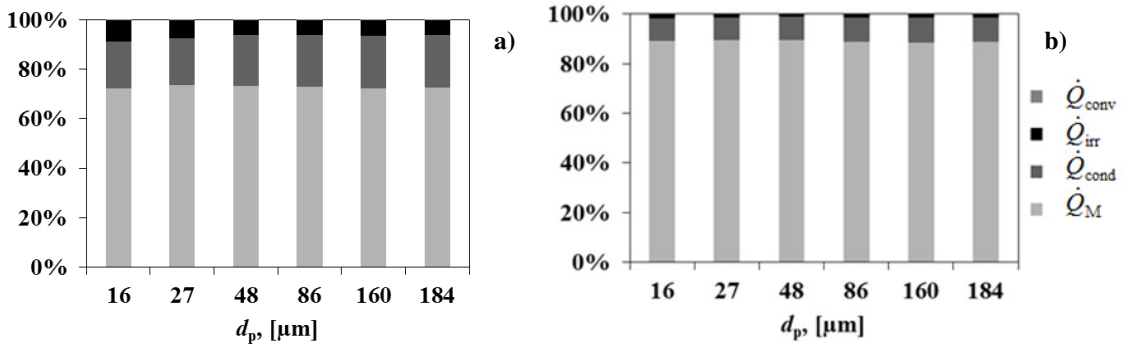

Figure 11. Energy partitioning for the different powder samples and for the different laser scan velocities: a) 1 mm s^{-1}; b) 5 mm s^{-1}.

4. Conclusions

SLS / SLM experiments carried out at different mean particle size and different laser speed indicate a change in the melted mass. as expected the melted mass increases at decreasing laser velocities. A local maximum of the ability of the laser to melt the granular material was found at about 48 µm mean particle size of the sample. It can be speculated that this is result is probably due to a different capacity of the granular material to absorb the IR radiation with a wavelength of 10.6 µm at different particle sizes. The bed effective conductivity, necessary for the heat balance on the melted mass and calculated according to Yagui and Kunni [12], was validated with a transint temperature experimental procedure. The energy balance applied to the experimental data indicate decreasing melted material temperature with particle size and, of course, with laser speed. The energy balance also indicated that the most significant heat dispersion term is bed conduction and that, increasing the laser scanning speed can considerably reduce thermal power dispersion and increase the effectiveness of the energy transfer provided by the laser beam.

References

[1] Tang, Y., Fuh, J.Y.H., Loh, H.T., Wong, Y.S., Lu, L. 2003 Direct laser sintering of a silica sand. Materials and Design 24, 623–629.
[2] Tian, X., Günster, J, Melcher, J., Li, D., Heinrich, J.G. 2009 Process parameters analysis of direct laser sintering and post treatment of porcelain components using Taguchi's method. J. Europ. Ceram. Soc. 29, 1903–1915.
[3] Ph. Bertrand, F. Bayle, C. Combe, P. Goeuriot, I. Smurov 2007 "Ceramic components manufacturing by selective laser sintering" Applied Surface Science in press.
[4] Nikolay K. Tolochko, et al. 2003. Mechanisms of selective laser sintering and heat transfer in Ti powder. Rapid Prototyping Journal, Vol. 9 Iss: 5 pp. 314-326.
[5] Lu Z.L., Li D.C., Lu B.H. 2010 The prediction of the building precision in the Laser Engineered Net Shaping process using advanced networks. Optics and Lasers in Engineering 48, 519–525.
[6] H.S.Carslaw, J.C.Jaeger 1959 "Conduction of Heat in Solids", Oxford University Press, Amen House, London E.C.4.
[7] Chen, T. and Y. Zhang 2006."Thermal modeling of laser sintering of two-component metal powder on top of sintered layers via multi-line scanning." Applied Physics A, Vol.86 iss:2 pp. 213-220.
[8] Chen, W.-L., Y.-C. Yang, et al. 2007. "Estimating the absorptivity in laser processing by inverse methodology." Applied Mathematics and Computation 190(1): 712-721.
[9] Meechoowas E., Tapasa K and Jitwatcharakomol T. 2013. Alternative Soda-lime Glass Batch to Reduce Energy Consumption Thailand Center of Excellence for Glass, Key Engineering Materials Vol. 545 pp 24-30.
[10] Roberts, I. A., C. J. Wang, et al. (2009), "A three-dimensional finite element analysis of the temperature field during laser melting of metal powders in additive layer manufacturing." International Journal of Machine Tools and Manufacture, Vol. 49 iss:12 pp. 916-923.
[11] Lloyd and Moran 1974 ASME Paper 74-WA/HT-66.
[12] Yagui, S. and Kunni, D. 1989 Studies on effective thermal conductivities in packed beds", J. AIChe., Vol. 3 No. 3, pp. 373-81.
[13] R. L. Rowley, W. V. Wilding, J. L. Oscarson, Y. Yang, N. A. Zundel, T. E. Daubert, R. P. Danner, 2007 DIPPR® Data Compilation of Pure Chemical Properties, Design Institute for Physical Properties, AIChE, New York.